A&A 591, A138 (2016)
DOI: 10.1051/0004-6361/201527722


Astronomy & Astrophysics

# Search for VHE gamma-ray emission from Geminga pulsar and nebula with the MAGIC telescopes

M. L. Ahnen[1], S. Ansoldi[2], L. A. Antonelli[3], P. Antoranz[4], A. Babic[5], B. Banerjee[6], P. Bangale[7], U. Barres de Almeida[7,25], J. A. Barrio[8], J. Becerra González[9,10,26], W. Bednarek[11], E. Bernardini[12,27], A. Berti[2,28], B. Biasuzzi[2], A. Biland[1], O. Blanch[13], S. Bonnefoy[8,⋆], G. Bonnoli[3], F. Borracci[7], T. Bretz[14,29], S. Buson[15], A. Carosi[3], A. Chatterjee[6], R. Clavero[9,10], P. Colin[7], E. Colombo[9,10], J. L. Contreras[8], J. Cortina[13], S. Covino[3], P. Da Vela[4], F. Dazzi[7], A. De Angelis[15], B. De Lotto[2], E. de Oña Wilhelmi[16], F. Di Pierro[3], M. Doert[17], A. Domínguez[8], D. Dominis Prester[5], D. Dorner[14], M. Doro[15], S. Einecke[17], D. Eisenacher Glawion[14], D. Elsaesser[17], V. Fallah Ramazani[18], A. Fernández-Barral[13], D. Fidalgo[8], M. V. Fonseca[8], L. Font[19], K. Frantzen[17], C. Fruck[7], D. Galindo[20], R. J. García López[9,10], M. Garczarczyk[12], D. Garrido Terrats[19], M. Gaug[19], P. Giammaria[3], N. Godinović[5], A. González Muñoz[13], D. Gora[12], D. Guberman[13], D. Hadasch[21], A. Hahn[7], Y. Hanabata[21], M. Hayashida[21], J. Herrera[9,10], J. Hose[7], D. Hrupec[5], G. Hughes[1], W. Idec[11], K. Kodani[21], Y. Konno[21], H. Kubo[21], J. Kushida[21], A. La Barbera[3], D. Lelas[5], E. Lindfors[18], S. Lombardi[3], F. Longo[2,28], M. López[8,⋆], R. López-Coto[13,30,⋆], P. Majumdar[6], M. Makariev[22], K. Mallot[12], G. Maneva[22], M. Manganaro[9,10], K. Mannheim[14], L. Maraschi[3], B. Marcote[20], M. Mariotti[15], M. Martínez[13], D. Mazin[7,31], U. Menzel[7], J. M. Miranda[4], R. Mirzoyan[7], A. Moralejo[13], E. Moretti[7], D. Nakajima[21], V. Neustroev[18], A. Niedzwiecki[11], M. Nievas Rosillo[8], K. Nilsson[18,32], K. Nishijima[21], K. Noda[7], L. Nogués[13], A. Overkemping[17], S. Paiano[15], J. Palacio[13], M. Palatiello[2], D. Paneque[7], R. Paoletti[4], J. M. Paredes[20], X. Paredes-Fortuny[20], G. Pedaletti[12], M. Peresano[2], L. Perri[3], M. Persic[2,33], J. Poutanen[18], P. G. Prada Moroni[23], E. Prandini[1,34], I. Puljak[5], I. Reichardt[15], W. Rhode[17], M. Ribó[20], J. Rico[13], J. Rodriguez Garcia[7], T. Saito[21,⋆], K. Satalecka[12], C. Schultz[15], T. Schweizer[7], S. N. Shore[23], A. Sillanpää[18], J. Sitarek[11], I. Snidaric[5], D. Sobczynska[11], A. Stamerra[3], T. Steinbring[14], M. Strzys[7], T. Surić[5], L. Takalo[18], F. Tavecchio[3], P. Temnikov[22], T. Terzić[5], D. Tescaro[15], M. Teshima[7,31], J. Thaele[17], D. F. Torres[24], T. Toyama[7], A. Treves[2], G. Vanzo[9,10], V. Verguilov[22], I. Vovk[7], J. E. Ward[13], M. Will[9,10], M. H. Wu[16], and R. Zanin[20,30]

*(Affiliations can be found after the references)*

Received 10 November 2015 / Accepted 27 February 2016

**ABSTRACT**

The Geminga pulsar, one of the brighest gamma-ray sources, is a promising candidate for emission of very-high-energy (VHE > 100 GeV) pulsed gamma rays. Also, detection of a large nebula has been claimed by water Cherenkov instruments. We performed deep observations of Geminga with the MAGIC telescopes, yielding 63 h of good-quality data, and searched for emission from the pulsar and pulsar wind nebula. We did not find any significant detection, and derived 95% confidence level upper limits. The resulting upper limits of $5.3 \times 10^{-13}$ TeV cm$^{-2}$ s$^{-1}$ for the Geminga pulsar and $3.5 \times 10^{-12}$ TeV cm$^{-2}$ s$^{-1}$ for the surrounding nebula at 50 GeV are the most constraining ones obtained so far at VHE. To complement the VHE observations, we also analyzed 5 yr of Fermi-LAT data from Geminga, finding that the sub-exponential cut-off is preferred over the exponential cut-off that has been typically used in the literature. We also find that, above 10 GeV, the gamma-ray spectra from Geminga can be described with a power law with index softer than 5. The extrapolation of the power-law *Fermi*-LAT pulsed spectra to VHE goes well below the MAGIC upper limits, indicating that the detection of pulsed emission from Geminga with the current generation of Cherenkov telescopes is very difficult.

**Key words.** astroparticle physics – stars: neutron – pulsars: general

## 1. Introduction

Geminga is the first known radio-quiet pulsar and the second brightest persistent source in the GeV sky. A review on the historical observations of Geminga can be found in Bignami & Caraveo (1996). Its light curve exhibits two peaks, hereafter P1 and P2, separated by 0.5 in phase. Gamma-ray emission from the interpulse region between P1 and P2 was reported by Fierro et al. (1998). The period of Geminga ($P \sim 237$ ms; Halpern & Holt 1992) and its derivative ($\dot{P} \sim 1.1 \times 10^{-14}$ s/s) correspond to a spin-down age of $\tau \sim 340$ kyr, a spin-down power $\dot{E}_{\rm rot} = 3.3 \times 10^{34}$ erg s$^{-1}$ and a surface magnetic field $B_{\rm surf} \sim 1.6 \times 10^{12}$ G. Although its spin-down luminosity is not as high as that of Crab and Vela, the short distance to this source makes the spin-down flux very high, which results in a high gamma-ray flux.

⋆ Corresponding authors: S. Bonnefoy, e-mail: simon@gae.ucm.es; M. López, e-mail: marcos@gae.ucm.es; R. López-Coto, e-mail: rlopez@ifae.es; T. Saito, e-mail: tysaito@cr.scphys.kyoto-u.ac.jp

The mechanism of gamma-ray emission of pulsars is not yet fully understood. Several emission locations were proposed as the origin of high-energy photons. The polar cap region (Sturrock 1971; Harding et al. 1978; Daugherty & Harding 1982), located close to the neutron star surface in the open magnetosphere, was the first to be proposed. However, a spectrum exhibiting a super-exponential cut-off at a few GeV is expected from the polar-cap gamma-ray emisson as a result of the magnetic pair creation. The proposed second region is the slot gap, located near the last open field line, which extends from the neutron star surface to the null surface (Arons 1983; Dyks & Rudak 2003; Muslimov & Harding 2004). The third proposed location of gamma-ray production is the outer gap (Cheng et al. 1986a,b; Romani & Yadigaroglu 1995), which is located along the last open field line and extends from the null surface to the light cylinder. The recent observations of the Crab pulsar at VHE by VERITAS and MAGIC (Aliu et al. 2011; Aleksić et al. 2011, 2012, 2014) require a new model to explain the emission above 100 GeV and the recent observation of pulsed emission above 400 GeV that extends beyond TeV energies, as reported recently by MAGIC (Ansoldi et al. 2016) challenges the theoretical models even more. An extension of the outer-gap model has been proposed (Lyutikov et al. 2012; Hirotani 2015) in which the emission is explained by magnetospheric cascades inside the gap. Recently, synchroton self-Compton emission from pairs was proposed to explain the emission from Crab, Vela and millisecond pulsars (Harding & Kalapotharakos 2015). The pairs are created above the polar cap and absorb radio photons which increases their perpendicular momentum. Another emission region, located at several light-cylinder radii, was investigated by Bogovalov & Aharonian (2000) and Aharonian et al. (2012), where the pulsed X-ray photons are inverse Compton up-scattered by a cold ultra-relativistic pulsar wind of electrons.

Geminga was first detected as an unidentified gamma-ray source by the *SAS-2* satellite (Fichtel et al. 1975). In 1977, the COS B satellite (Hermsen et al. 1977) confirmed gamma-ray emission from the same region. In 1983 an X-ray counterpart of the COS B source was observed (Bignami et al. 1983) and given the name Geminga, and in 1987 the optical counterpart was detected (Bignami et al. 1987). The X-ray pulsation was discovered by the ROSAT experiment (Halpern & Holt 1992) and was further observed in gamma rays by the EGRET telescope (Bertsch et al. 1992) onboard the *Compton* Gamma-Ray Observatory and COS B (Bignami & Caraveo 1992). The first time-period derivative was estimated using COS B data (Bignami & Caraveo 1992). In 1981, the spectrum of Geminga was measured by the COS B satellite (Masnou et al. 1981). It was characterized by a simple power-law function from 100 MeV up to a few GeV. The power-law spectrum was later confirmed by EGRET (Mayer-Hasselwander et al. 1994) with a harder index. The distance to the Geminga pulsar was first calculated by studying the interstellar absorption and proper motion, and was estimated to be approximately 100 pc (Bignami et al. 1983, 1993). A deeper study of the interstellar absorption that took the spin-down properties of the pulsar into account, set limit to the distance of Geminga of $250^{+150}_{-100}$ pc (Halpern & Ruderman 1993). Observations with the *Hubble* Space Telescope of the annual paralax led to more stringent constraint of the distance of $157^{+59}_{-30}$ pc (Caraveo et al. 1996).

Event though the Geminga pulsar is radio quiet, several investigations were carried out to search for radio emission. A detection at 102.5 MHz was claimed in 1997 (Malofeev & Malov 1997) with a flux varying between 5 and 500 mJy. Strong variations in the emission and pulse widths were reported as well. A soft spectrum would explain the absence of detected pulsed emission above 102 MHz. Recently, pulsed emission from the Geminga pulsar was reported at 42, 62 and 111 MHz (Malov et al. 2015). Based on these recent observations, the previous radio silence from the Geminga pulsar has been interpreted as a long-term variability of the radio emission with a period of several years.

The Geminga pulsar, with one of the highest fluxes detected in the gamma-ray band (Acero et al. 2015; $4.5 \times 10^{-9}$ erg cm$^{-2}$ s$^{-1}$ above 100 MeV) and a spectrum extending above 25 GeV, is a good candidate to be detected by Cherenkov telescopes. The detection of the Geminga pulsar with the MAGIC telescopes and the characterization of its timing and spectral features can shed light on the emission location and mechanisms at work in such an old pulsar.

One year of *Fermi*-Large Area Telescope (LAT; Atwood et al. 2009) observations at high energies resulted in a power-law spectrum with an exponential cut-off at (2.5 ± 0.2) GeV (Abdo et al. 2010b). The study of the phase-resolved emission with fine binning shows a strong dependency of the cut-off energy on the phase region considered. The pulsation is still clearly seen above 10 GeV with a reported significance greater than $6\sigma$, using three years of data, and a hint was observed above 25 GeV (Ackermann et al. 2013).

The spectral shape and the pulsed emission above 25 GeV rules out the polar-cap model, in which a super-exponential cut-off is expected at a few GeV. The *Fermi*-LAT collaboration also reported that the peak intensity of P2 increases relative to the peak intensity of P1 above 200 MeV (Abdo et al. 2010b). Recently the VERITAS collaboration reported about the search for VHE emission from the Geminga pulsar, in which no signal was detected above 100 GeV (Aliu et al. 2015). They computed upper limits of $4.0 \times 10^{-13}$ cm$^{-2}$ s$^{-1}$ and $1.7 \times 10^{-13}$ cm$^{-2}$ s$^{-1}$ on the integrated flux above 135 GeV for P1 and P2, respectively, using a spectral index of −3.8. The second catalog of hard *Fermi*-LAT sources (2FHL; Ackermann et al. 2016) does not mention a detection of Geminga above 50 GeV either.

In addition to the emission from the pulsar, an X-ray nebula was discovered around the Geminga pulsar (Caraveo et al. 2003). It shows an extended structure that is aligned with the pulsar proper motion direction (Bignami et al. 1993). Observations with the *Chandra* and *XMM-Newton* satellites (de Luca et al. 2006; Pavlov et al. 2006) reported the detection of three tail-like structures behind the pulsar; one 25″ tail aligned with the pulsar proper motion, and two 2′ outer tails. Another 50″ emitting region ahead of the pulsar was reported.

At gamma-ray energies, the *Fermi*-LAT reported a continuous emission over the whole pulsar rotation, but this is incompatible with a surrounding nebula (Abdo et al. 2010b). The Whipple collaboration obtained an integral flux upper limit for continuous emission of $8.8 \times 10^{-12}$ cm$^{-2}$ s$^{-1}$ above 0.5 TeV (Akerlof et al. 1993). At higher energies, the Milagro collaboration reported the detection of a TeV extended steady emission from Geminga at a significance of $6.3\sigma$, recently confirmed by HAWC (Baughman et al. 2015). Milagro observed an emission region that is extended by 2–3 deg and reported a flux level of $(38 \pm 11) \times 10^{-17}$ TeV$^{-1}$ cm$^{-2}$ s$^{-1}$ at 35 TeV (Abdo et al. 2009). At radio frequencies, many observers have attempted to detect a continuous emission from Geminga. Only the deepest VLA interferometric observation of Geminga performed in 2004 (Giacani et al. 2005), resulted in the detection of steady radio emission. Overall, the Geminga radio tail is compatible with the scenario of a synchrotron-emitting PWN.

To study the gamma-ray emission of the Geminga pulsar and nebula, we collected 75 h of observation with MAGIC. Furthermore, we analyzed five years of *Fermi*-LAT data to complement the VHE observations.

## 2. MAGIC observations and data analysis

The MAGIC telescopes are a set of two imaging atmospheric Cherenkov telescopes. They are located at a height of 2200 m a.s.l. in the Roque de los Muchachos Observatory, on La Palma island (Spain). Both telescopes consist of a 17 m diameter reflector and a fast-imaging camera with a field of view of 3.5° diameter. The trigger threshold for standard observations at zenith angles below 35° is around 50 GeV. The MAGIC telescopes have an integral sensitivity of 0.66% of the Crab nebula flux above 220 GeV for 50 h of observation, with an angular resolution of ~0.07° and an energy resolution of 16% (Aleksić et al. 2016b).

Observations of the Geminga pulsar and nebula were performed between December 2012 and March 2013, with the upgraded MAGIC telescopes (Aleksić et al. 2016a). During this period, a total of ~75 h were taken at zenith angles below 35° to ensure the lowest possible energy threshold. The observations were performed in the so-called wobble mode (Fomin et al. 1994), where the source is offset by 0.4° from the camera center. After rejecting data taken under unfavorable weather or technical conditions, 63 h of data remained for the analysis. Together with each event image, we recorded the absolute event arrival time using a GPS receiver. The performance of the MAGIC time acquisition system was evaluated by periodically observing the Crab pulsar in the optical wave band with a special PMT located at the MAGIC camera center (Lucarelli et al. 2008).

The data analysis was performed using the standard MAGIC analysis chain MARS (Zanin et al. 2013). The phase of the events was computed using *tempo2* (Hobbs et al. 2006). The ephemeris was provided by the *Fermi*-LAT collaboration[1] (Ray et al. 2011). For the pulsar analysis, gamma-ray candidate events were selected by applying cuts in hadronness and in $\theta^2$. Hadronness is a particle-identification estimator that classifies events into gamma-ray or hadron candidates, while $\theta^2$ is the squared angular distance between the source position and the re-constructed source position. The cuts are optimized using a background sample and Monte Carlo gamma-ray sample by maximizing the $Q$-factor in each energy bin. This is defined as: $Q = \varepsilon_{\rm on}/\sqrt{\varepsilon_{\rm off}}$, where $\varepsilon_{\rm on}$ and $\varepsilon_{\rm off}$ are the efficiency of the cuts for signal and background data, respectively. To compute the cuts we imposed that at least 50% of the Monte Carlo gamma-ray events survive the cuts. The significance of the pulsed emission was estimated using Eq. (17) in Li & Ma (1983). The upper limits on the pulsed emission were computed using the Rolke method (Rolke & López 2001) assuming a Poissonian background and requiring a 95% confidence level.

The search for a steady extended emission was made by computing the signal-to-noise ratio around the Geminga pulsar. Several extensions around the Geminga pulsar were considered, by setting different values of the cut in $\theta^2$ (0.04, 0.06, 0.08 and 0.1 deg$^2$). We also produces a significance sky map of the region around the Geminga pulsar. The significance in each bin of the sky map was computed using the Li & Ma method applied on a background estimate. The cuts were selected by maximizing the $Q$-factor on a contemporaneous Crab nebula sample using the hadronness and size parameters of the images, which is defined as the sum of the charge from each pixel. The upper limits for the nebula emission were computed using the same method as for the pulsed emission and different spectral assumption.

[1] http://www.slac.stanford.edu/~kerrm/fermi_pulsar_timing/J0633+1746/html/J0633+1746_54683_56587_chol.par

**Table 1.** Definition of the signal and off-pulse regions derived from the LAT data.

| P1 | P2 | Off-region |
|---|---|---|
| 0.066–0.118 | 0.565–0.607 | 0.7–0.95 |

## 3. *Fermi*-LAT observation

### 3.1. Fermi data analysis

A data sample of five years (from 54 710 up to 56 587 MJD) of *Fermi*-LAT data was analyzed. We analyzed this data-set using the P7REP_SOURCE_V15 instrument response functions and the *Fermi* tools version v9r31p1. We selected events that were recorded when the telescope was in nominal science mode and when the rocking angle was lower than 52°. To reject the background coming from the Earth's limb, we selected photons with a zenith angle ≤100°. The phase and barycentric corrections of the events were computed using *tempo2* with the same ephemeris as for MAGIC data. We computed the light curve and the spectral energy distribution for the two peaks, P1 and P2, separately. Furthermore, we calculated the phase-averaged (PA) emission. The pulsar light curve was produced using an energy-dependent region of interest (ROI) with a radius defined as $R = \max(6.68 - 1.76 \times \log(E), 1.3)°$ as in Abdo et al. (2010a).

For the spectral analysis, the binned likelihood method was used. We set the ROI to 15° as in Abdo et al. (2013). We included all the sources from the third *Fermi* catalog (Acero et al. 2015) in the background model. For sources with a significance higher than $5\sigma$ that were located at less than 10 deg away from the Geminga pulsar, only the normalization factor was left free. We also let the normalization factor of the isotropic and Galactic background models free. We discarded all the sources with TS < 2. For all the remaining sources all the parameters were fixed to the catalog values. To calculate the spectral points, we repeated the procedure in each energy bin using a power law with the spectral index and normalization factor free to vary. Only spectral points with a significance higher than $2\sigma$ are shown in the plots.

### 3.2. Fermi-LAT results

We computed the light curve above 100 MeV. To determine the pulses profiles and OFF phase range we used photons with energy higher than 5 GeV for P1 and higher than 10 GeV for P2. The two different energy ranges are motivated by the aim of evaluating the peak shape at the highest energy to achieve a better match with the shape we would expect at the MAGIC energy range, maintaining enough statistics. We fit both peaks to asymmetric Gaussian functions. We used as signal region the peak position $\pm 1\sigma$, as shown in Table 1. We defined the background region in the off-phase where no emission is expected from the pulsar. From now on P1 and P2 are referred to with the values in Table 1. The obtained light curve above 100 MeV together with the signal and background regions are shown in Fig. 1 together with a close-up on the fits of P1 and P2 at the corresponding energies.

We fit the spectral energy distribution (SED) of P1, P2 and the PA using two different spectral shapes: a power-law with an

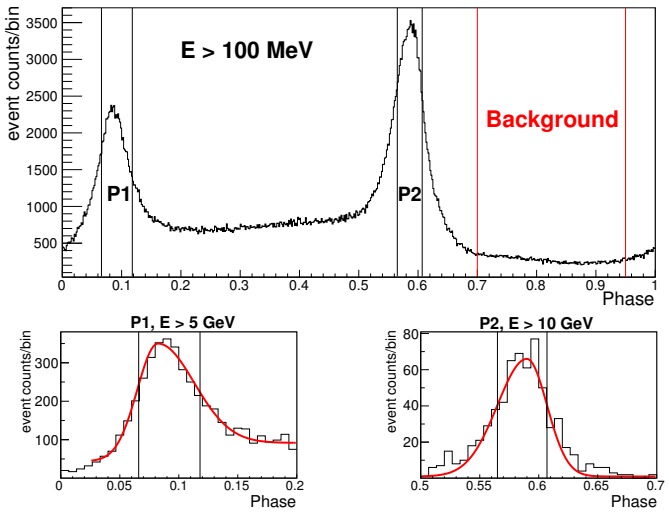


**Fig. 1.** Light curve computed with the *Fermi*-LAT data above 100 MeV (*top*). A close-up is made on both P1 above 5 GeV and P2 above 10 GeV and their corresponding Gaussian fits (*bottom*), with resulting $\chi^2$/d.o.f values of 61/26 and 32/29 for P1 and P2, respectively. The vertical black lines define the signal regions, while the vertical red lines define the off-pulse region used to determine the background.

**Table 2.** Spectral parameters of the fit using the likelihood method for the SEC function between 100 MeV and 100 GeV for P1, P2 and PA.

| | $N_0$ | $\alpha$ | $E_c$ [GeV] | $b$ |
|---|---|---|---|---|
| P1 | $3.0 \pm 0.3$ | $1.12 \pm 0.04$ | $1.2 \pm 0.1$ | $0.81 \pm 0.04$ |
| P2 | $4.3 \pm 0.4$ | $0.78 \pm 0.03$ | $1.1 \pm 0.1$ | $0.70 \pm 0.03$ |
| PA | $28.3 \pm 1.8$ | $0.94 \pm 0.02$ | $0.8 \pm 0.1$ | $0.67 \pm 0.02$ |

**Notes.** The normalization factor, $N_0$, is given in units of $10^{-10}$ MeV$^{-1}$ s$^{-1}$ cm$^{-2}$. The quoted errors are statistical at a $1\sigma$ confidence level. The systematic errors reported by the *Fermi*-LAT are of 14% on $\alpha$ and 4% on $E_c$ (Abdo et al. 2013).

exponential cut-off function (EC), and a power-law with a sub-exponential cut-off function (SEC). The sub-exponential ($b < 1$) and exponential ($b = 1$) cut-off functions are defined by the following equation:

$$\frac{dF}{dE} = N_0 \left(\frac{E}{E_0}\right)^{-\alpha} \exp(-(E/E_c)^b), \quad (1)$$

where $E_0$ is the energy scale, set to 927.9 MeV as computed in Acero et al. (2015), $\alpha$ the spectral index, and $E_c$ the cut-off energy. The results of the computed spectra using a SEC function are shown in Table 2.

To characterize the emission at high energies, we fit the high-energy tail (above 10 GeV) for P1 and P2 using a power law. The normalization factors were computed at 10 GeV. The results of the power-law fit above 10 GeV are shown in Table 3.

The resulting spectra computed using five years of *Fermi*-LAT data are consistent with the previous results reported by the Fermi-LAT collaboration (Abdo et al. 2010b, 2013). The SEC appears to agree better with the data. The $b$ parameter, indicating how much the data deviate from an EC is significantly smaller than one. The calculation of the likelihood ratio of the SEC model over EC also results in a deviation for the SEC of $6\sigma$, $11\sigma$ and $24\sigma$ for P1, P2 and PA, respectively. We also computed the SED using finer binning to estimate the evolution of the $b$ parameter according to the phase width considered. The

**Table 3.** Results of the fit of P1 and P2 spectral energy distribution with a power law above 10 GeV.

| | $N_0$ | $\alpha$ |
|---|---|---|
| P1 | $(5.9 \pm 1.4) \times 10^{-5}$ | $5.3 \pm 0.7$ |
| P2 | $(7.2 \pm 0.1) \times 10^{-4}$ | $5.2 \pm 0.3$ |

**Notes.** The normalization factor, $N_0$, is given in unit of $10^{-9}$ MeV$^{-1}$ s$^{-1}$ cm$^{-2}$.

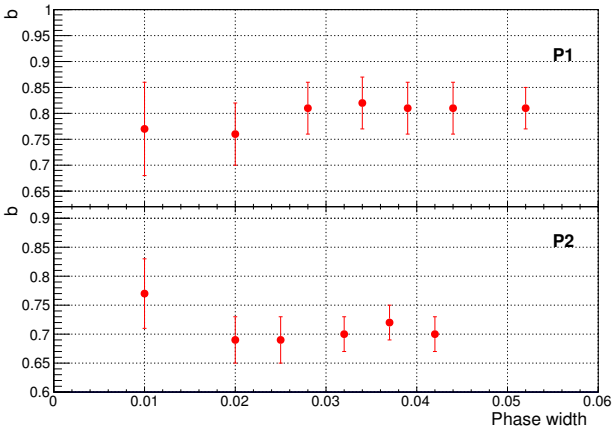


**Fig. 2.** Computation of the sub-exponential cut-off $b$ parameter according to the phase width considered for P1 (*top*) and P2 (*bottom*).

top and bottom panels in Fig. 2 represent the value computed for P1 and P2, respectively. The smallest width was taken as 0.01 in phase because we lack statistics for smaller regions. We did not observe any significant variation of $b$ with the pulse width.

## 4. MAGIC results

We computed the light curve and the corresponding significances for the pulsed emission in three energy ranges: above 50 GeV, 50–100 GeV and 100–200 GeV, as shown in Fig. 3. The background was estimated from the off-pulse region (gray area; phase 0.70–0.95) and the dashed red line represents the averaged number of events in the background region. We computed the significance for P1, P2, and the sum of both peaks. The results of the statistical tests are shown in Table 4. No significant pulsation was found in MAGIC data in any of the energy ranges investigated. We computed the upper limits for the pulsed emission. The spectral indices used for the upper limits computation were obtained from the extrapolation of P1 and P2 *Fermi*-LAT spectra above 10 GeV using a power law (see Table 3).

The differential upper limits computed for the pulsed emission are shown in Fig. 4 by the black arrows. The black lines above the arrows indicate the spectral slope used for the upper limit computations. The dot-dot-dashed blue line represents the fit to *Fermi* data above 10 GeV with a power-law function, the dashed line the result of the fit of the SED to a SEC and the dot-dashed line the result of the fit of the SED to an EC. The statistical error contour is also plotted for the power-law fits at high energies.

Figure 5 shows the sky map of the signal significance around the Geminga pulsar for the steady emission using MAGIC data. The position of the Geminga pulsar is marked with a cross. The white circle represents the standard deviation of the Gaussian function used for the smearing of the sky map. No significant

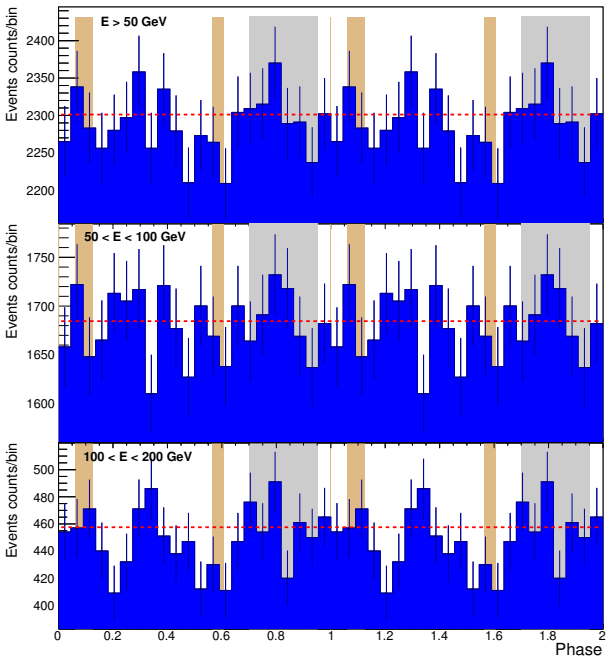


**Fig. 3.** Light curves of the Geminga pulsar obtained with MAGIC for different energy bins. *From top to bottom*: above 50 GeV, 50–100 GeV and 100–200 GeV. Two cycles are plotted for clarity. The bin width corresponds to ∼10.8 ms (1/22 of the Geminga rotational period). The shaded brown areas show the positions of P1 (main pulse) and P2 (interpulse). The gray area shows the off-region. The dashed red line represents the averaged number of events in the background region.

**Table 4.** Significance computed for P1, P2 and the sum of both peaks.

| Energy range (GeV) | P1 | P2 | P1 + P2 |
|---|---|---|---|
| ≥50 | $0.2\sigma$ | $-0.1\sigma$ | $0.1\sigma$ |
| 50–100 | $-0.2\sigma$ | $0.2\sigma$ | $0.0\sigma$ |
| 100–200 | $0.7\sigma$ | $-1.4\sigma$ | $-0.3\sigma$ |

**Notes.** The significances were computed using Li & Ma (1983).

emission was found from the Geminga nebula above 50 GeV. We calculated the differential upper limits on the emission from the nebula surrounding the Geminga pulsar in the energy range covered by MAGIC. The computed differential upper limits are represented by the black arrows in Fig. 6. The spectral index used to compute the upper limit was taken as −2.6. To estimate the upper limit variations that are due to assuming the spectral index value, we recomputed the upper limits assuming two different spectral indices of −2.0 and −2.8. The two chosen values define the typical range of spectral indices for pulsar wind nebulae (Strakovsky & Blokhintsev 2013). A fluctuation of 13% is observed in the upper limit computation below 120 GeV. For energies above 120 GeV the variations are below 10%. We also estimated the integral upper limits on the emission from the nebula to be $2.4 \times 10^{-11}$ cm$^{-2}$ s$^{-1}$ and $3.2 \times 10^{-12}$ cm$^{-2}$ s$^{-1}$ above 50 GeV and 200 GeV, respectively. In Fig. 6, the computed PA SED using five years of *Fermi*-LAT data is represented by black points. The dashed blue lines are the result of computing the *Fermi* spectral shape using a power law with a sub-exponential cut-off, the dot-dashed line shows the same using a power-law with an exponential cut-off. The green point represents the flux level of the Geminga nebula as seen by MILAGRO (Abdo et al. 2009).

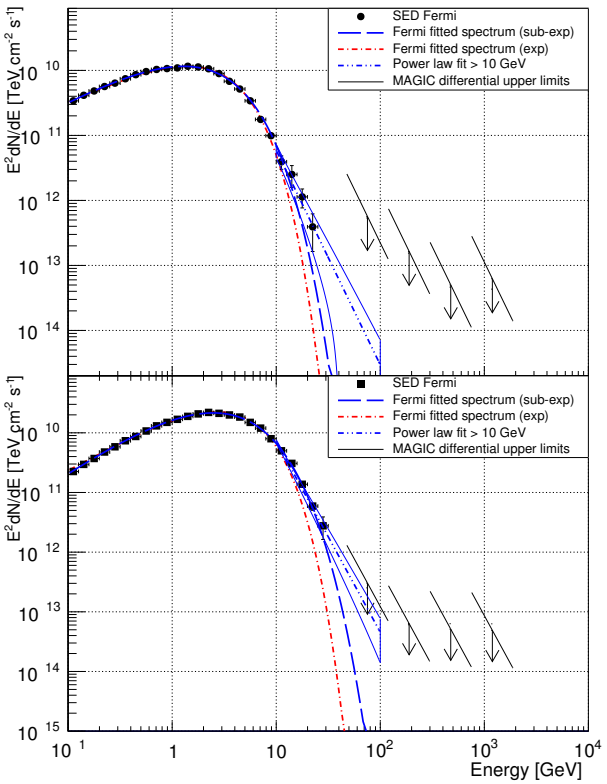


**Fig. 4.** P1 (*top*) and P2 (*bottom*) SED. The differential upper limits are represented by the black arrows. The blue dashed line represents the SED computed using five years of *Fermi*-LAT data assuming a SEC function, between 100 MeV and 100 GeV, and the dot-dashed line the fit of SED to an EC function. The dot-dot-dashed line is the result of the fit of the *Fermi* data above 10 GeV with a power law. The statistical error contour from the power-law fit is also plotted.

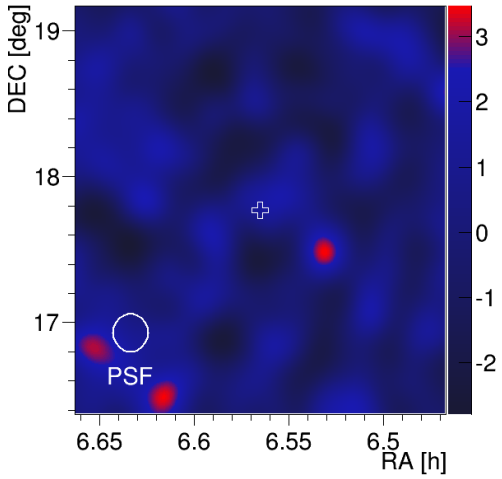


**Fig. 5.** Sky map representing the signal significance computed around the location of the Geminga pulsar using MAGIC data above 50 GeV. The cross at the center of the map represents the Geminga pulsar location. The white circle represents the function used to deconvolve the sky map.

## 5. Discussion and conclusions

During the winter 2012/13 (from December 2012 to March 2013), the Geminga pulsar and its surrounding nebula were observed by the MAGIC telescopes. 63 h were selected

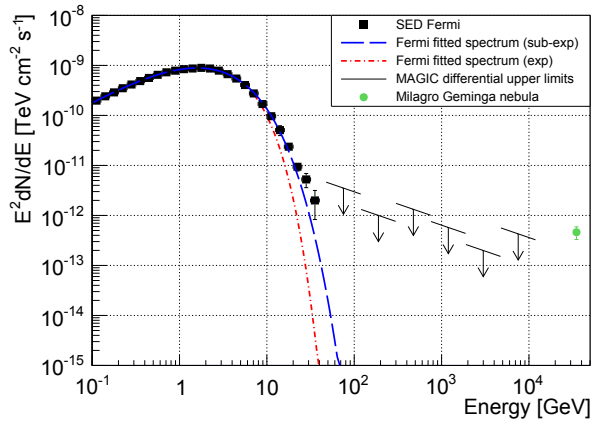


**Fig. 6.** Phase-averaged spectral energy distribution. The differential upper limits are represented by the black arrows. The blue dashed line represents the SED computed using five years of *Fermi*-LAT data assuming a SEC function, between 100 MeV and 100 GeV. The green point represents the flux level of the Geminga nebula as seen by MILAGRO.

for their good quality to search for emission from the pulsar and its surrounding nebula at VHE. The analysis of the MAGIC data yielded no significant signal and hence resulted in the computation of upper limits above 50 GeV for both pulsed and steady emission. In addition to MAGIC data, five years of *Fermi*-LAT data were analyzed to derive pulsed and phase-averaged emission and compare them to the VHE upper limits. Our results on the analysis of MAGIC and *Fermi*-LAT data are consistent with those reported in the 2FHL, where no significant signal from Geminga was found above 50 GeV. In addition, the computed integral upper limit on the emission from the nebula above 200 GeV is compatible with the flux level reported by Milagro.

The *Fermi*-LAT spectra from 0.1 GeV to 30 GeV can be described by a power law with a sub-exponential cut-off. As reported by Lyutikov (2012), a simple power law can also be used to characterize the emission at high energies, and more statistics would be required to distinguish between the spectral shapes. The upper limits computed using the MAGIC data are well above the *Fermi*-LAT power-law spectra extrapolated to VHE, and hence they do not provide additional constraints on the spectral shape of the pulsed emission. Therefore, the mechanism responsible for the high-energy emission from the Geminga pulsar is difficult to establish. At high energies, the emission due to synchro-curvature radiation and inverse Compton scattering are expected to exhibit different spectral shapes. For example, in the framework of the outer-gap model, where the high-energy emission takes place at high altitudes from the neutron star (Cheng et al. 1986a,b), a curvature or synchro-curvature radiation mechanism would exhibit a spectral shape that is well characterized by an exponential cut-off (Prosekin et al. 2013; Viganò & Torres 2015). As the radiation is very sensitive to the pitch angle of the radiating particles, the sum of the emission from particles with the same energy but different angles results in a less abrupt cut-off. Furthermore, calculations of the outer-gap magnetic-field-aligned electric field evolution (Hirotani 2006, 2015) show that the accelerating electric field depends on the height in the gap and reaches a maximum in the center of the gap. Distinct heights with different values of the electric field would accelerate particles at different energies, resulting in a spread of the cut-off energy values. A strong dependency of the cut-off energy on the accelerating electric field is reported by Viganò et al. (2015). This behavior of the cut-off values was reported for the Geminga pulsar (Abdo et al. 2010b). The Fermi collaboration studied the phase-resolved evolution of the cut-off energy for the Geminga pulsar over the whole pulsar rotation using bin sizes where each bin contained 2000 photons. The results show that within the P1 and P2 phase regions, where the computed cut-off values are the highest, these values vary. Considering wider phase ranges, the fluctuations of the cut-off value would result in an a sub-exponential cut-off spectral shape. However, the pulsed gamma-ray spectra we computed using fine bins in phase around the pulses' positions discard the exponential cut-off because the best-fit values for the $b$ parameter are significantly lower than 1. For synchro-curvature radiation, this deviation can arise from the caustic emission (Dyks & Rudak 2003), that is overlapping of photons emitted at different heights and along different magnetic field lines. If the caustic effect were more important for P2 than P1 as a result of the curvature of the magnetic field line, the greater values of $b$ for P1 with respect to P2 would be explained.

For an inverse Compton (IC) emission or synchroton self-Compton within the outer gap (Hirotani 2015), the break in the spectral shape would correspond to a break in the particle distribution function (Lyutikov 2012) if all the emission comes from this mechanism. If the particles are distributed as a broken power law, then the IC spectrum would appear as a broken power law as well, and a high-energy power-law-like tail would be seen, as it is the case for the Crab pulsar (Aliu et al. 2011; Aleksić et al. 2011, 2012, 2014; Ansoldi et al. 2016). However, for an inverse Compton emission, the power-law tail exhibited by the Geminga pulsar would be much softer than that of the Crab (Aleksić et al. 2014), as can be seen from the power-law spectral fit of the *Fermi*-LAT data above 10 GeV. A hard gamma-ray tail is not expected even if the curvature radiation is produced in a curved magnetic field close to the light cylinder (Bednarek 2012).

The analysis of the nebula around the Geminga pulsar shows no significant detection above 50 GeV. The presence of the nebula is unknown at the GeV scale. Indeed, observations of the Geminga pulsar with the *Fermi*-LAT show no evidence of a surrounding nebula. The detection of a large nebula similar to the one claimed by the Milagro Collaboration is not straightforward for MAGIC, as its extension is larger than the field of view of the telescopes. Overall, the prospects of detecting the Geminga pulsar with the current Cherenkov telescopes are rather low. However, the upcoming Cherenkov Telescope Array (CTA; Bernlöhr et al. 2013) could, with a better sensitivity and a lower energy threshold, detect high-energy gamma-ray emission from the Geminga pulsar and thus shed light on the physics of pulsars. We have estimated that Geminga could be detected at a $5\sigma$ level by CTA in 50 h.

*Acknowledgements.* We would like to thank the Instituto de Astrofísica de Canarias for the excellent working conditions at the Observatorio del Roque de los Muchachos in La Palma. The financial support of the German BMBF and MPG, the Italian INFN and INAF, the Swiss National Fund SNF, the ERDF under the Spanish MINECO (FPA2012-39502), and the Japanese JSPS and MEXT is gratefully acknowledged. This work was also supported by the Centro de Excelencia Severo Ochoa SEV-2012-0234, CPAN CSD2007-00042, and MultiDark CSD2009-00064 projects of the Spanish Consolider-Ingenio 2010 programme, by grant 268740 of the Academy of Finland, by the Croatian Science Foundation (HrZZ) Project 09/176 and the University of Rijeka Project 13.12.1.3.02, by the DFG Collaborative Research Centers SFB823/C4 and SFB876/C3, and by the Polish MNiSzW grant 745/N-HESS-MAGIC/2010/0.

## References

Abdo, A. A., Allen, B. T., Aune, T., et al. 2009, ApJ, 700, L127
Abdo, A. A., Ackermann, M., Ajello, M., et al. 2010a, ApJ, 708, 1254
Abdo, A. A., Ackermann, M., Ajello, M., et al. 2010b, ApJ, 720, 272
Abdo, A. A., Ajello, M., Allafort, A., et al. 2013, ApJS, 208, 17

Acero, F., Ackermann, M., Ajello, M., et al. 2015, ApJS, 218, 23
Ackermann, M., Ajello, M., Allafort, A., et al. 2013, ApJS, 209, 34
Ackermann, M., Ajello, M., Atwood, W. B., et al. 2016, ApJS, 222, 5
Aharonian, F. A., Bogovalov, S. V., & Khangulyan, D. 2012, Nature, 482, 507
Akerlof, C. W., Breslin, A. C., Cawley, M. F., et al. 1993, A&A, 274, L17
Aleksić, J., Alvarez, E. A., Antonelli, L. A., et al. 2011, ApJ, 742, 43
Aleksić, J., Alvarez, E. A., Antonelli, L. A., et al. 2012, A&A, 540, A69
Aleksić, J., Ansoldi, S., Antonelli, L. A., et al. 2014, A&A, 565, L12
Aleksić, J., Ansoldi, S., Antonelli, L. A., et al. 2016a, Astropart. Phys., 72, 61
Aleksić, J., Ansoldi, S., Antonelli, L. A., et al. 2016b, Astropart. Phys., 72, 76
Aliu, E., Arlen, T., Aune, T., et al. 2011, Science, 334, 69
Aliu, E., Archambault, S., Archer, A., et al. 2015, ApJ, 800, 61
Ansoldi, S., Antonelli, L. A., Antoranz, P., et al. 2016, A&A, 585, A133
Arons, J. 1983, ApJ, 266, 215
Atwood, W. B., Abdo, A. A., Ackermann, M., et al. 2009, ApJ, 697, 1071
Baughman, B. M., Wood, J., for the HAWC Collaboration 2015, Proc. of the 34th ICRC, The Hague, 2015 [arXiv:1508.03497]
Bednarek, W. 2012, MNRAS, 424, 2079
Bernlöhr, K., Barnacka, A., Becherini, Y., et al. 2013, Astropart. Phys., 43, 171
Bertsch, D. L., Brazier, K. T. S., Fichtel, C. E., et al. 1992, Nature, 357, 306
Bignami, G. F., & Caraveo, P. A. 1992, Nature, 357, 287
Bignami, G. F., & Caraveo, P. A. 1996, ARA&A, 34, 331
Bignami, G. F., Caraveo, P. A., & Lamb, R. C. 1983, ApJ, 272, L9
Bignami, G. F., Caraveo, P. A., Paul, J. A., Salotti, L., & Vigroux, L. 1987, ApJ, 319, 358
Bignami, G. F., Caraveo, P. A., & Mereghetti, S. 1993, Nature, 361, 704
Bogovalov, S. V., & Aharonian, F. A. 2000, MNRAS, 313, 504
Caraveo, P. A., Bignami, G. F., Mignani, R., & Taff, L. G. 1996, ApJ, 461, L91
Caraveo, P. A., Bignami, G. F., De Luca, A., et al. 2003, Science, 301, 1345
Cheng, K. S., Ho, C., & Ruderman, M. 1986a, ApJ, 300, 500
Cheng, K. S., Ho, C., & Ruderman, M. 1986b, ApJ, 300, 522
Daugherty, J. K., & Harding, A. K. 1982, ApJ, 252, 337
de Luca, A., Caraveo, P. A., Mattana, F., Pellizzoni, A., & Bignami, G. F. 2006, A&A, 445, L9
Dyks, J., & Rudak, B. 2003, ApJ, 598, 1201
Fichtel, C. E., Hartman, R. C., Kniffen, D. A., et al. 1975, ApJ, 198, 163
Fierro, J. M., Michelson, P. F., Nolan, P. L., & Thompson, D. J. 1998, ApJ, 494, 734
Fomin, V. P., Stepanian, A. A., Lamb, R. C., et al. 1994, Astropart. Phys., 2, 137
Giacani, E., Reynoso, E. M., Dubner, G., et al. 2005, Adv. Space Res., 35, 1070
Halpern, J. P., & Holt, S. S. 1992, Nature, 357, 222
Halpern, J. P., & Ruderman, M. 1993, ApJ, 415, 286
Harding, A. K., & Kalapotharakos, C. 2015, ApJ, 811, 63
Harding, A. K., Tademaru, E., & Esposito, L. W. 1978, ApJ, 225, 226
Hermsen, W., Swanenburg, B. N., Bignami, G. F., et al. 1977, Nature, 269, 494
Hirotani, K. 2006, Mod. Phys. Lett. A, 21, 1319
Hirotani, K. 2015, ApJ, 798, L40
Hobbs, G. B., Edwards, R. T., & Manchester, R. N. 2006, MNRAS, 369, 655
Li, T.-P., & Ma, Y.-Q. 1983, ApJ, 272, 317
Lucarelli, F., Barrio, J., Antoranz, P., et al. 2008, Nucl. Instr. Meth. Phys. Res. A, 589, 415
Lyutikov, M. 2012, ApJ, 757, 88
Lyutikov, M., Otte, N., & McCann, A. 2012, ApJ, 754, 33
Malofeev, V. M., & Malov, O. I. 1997, Nature, 389, 697
Malov, O. I., Malofeev, V. M., Teplykh, D. A., & Logvinenko, S. V. 2015, Astron. Rep., 59, 183
Masnou, J. L., Paul, J. A., Bennett, K., et al. 1981, Int. Cosmic Ray Conf., 1, 177
Mayer-Hasselwander, H. A., Bertsch, D. L., Brazier, K. T. S., et al. 1994, ApJ, 421, 276
Muslimov, A. G., & Harding, A. K. 2004, ApJ, 606, 1143
Pavlov, G. G., Sanwal, D., & Zavlin, V. E. 2006, ApJ, 643, 1146
Prosekin, A. Y., Kelner, S. R., & Aharonian, F. A. 2013, ArXiv e-prints [arXiv:1305.0783]
Ray, P. S., Kerr, M., Parent, D., et al. 2011, ApJS, 194, 17
Rolke, W. A., & López, A. M. 2001, Nucl. Instr. Meth. Phys. Res. A, 458, 745
Romani, R. W., & Yadigaroglu, I.-A. 1995, ApJ, 438, 314
Strakovsky, I., & Blokhintsev, I. 2013, The Universe Evolution: Astrophysical and Nuclear Aspects (Nova Science Pub. Inc.)
Sturrock, P. A. 1971, ApJ, 164, 529
Viganò, D., & Torres, D. F. 2015, MNRAS, 449, 3755
Viganò, D., Torres, D. F., & Martín, J. 2015, MNRAS, 453, 2599
Zanin, R., Carmona, E., Sitarek, J., et al. 2013, Proc. of the 33rd ICRC, Rio de Janeiro, 2013

[1] ETH Zurich, 8093 Zurich, Switzerland
[2] Università di Udine, and INFN Trieste, 33100 Udine, Italy
[3] INAF National Institute for Astrophysics, 00136 Rome, Italy
[4] Università di Siena, and INFN Pisa, 53100 Siena, Italy
[5] Croatian MAGIC Consortium, Rudjer Boskovic Institute, University of Rijeka, University of Split and University of Zagreb, Croatia
[6] Saha Institute of Nuclear Physics, 1/AF Bidhannagar, Salt Lake, Sector-1, 700064 Kolkata, India
[7] Max-Planck-Institut für Physik, 80805 München, Germany
[8] Universidad Complutense, 28040 Madrid, Spain
[9] Inst. de Astrofísica de Canarias, 38200 La Laguna, Tenerife, Spain
[10] Universidad de La Laguna, Dpto. Astrofísica, 38206 La Laguna, Tenerife, Spain
[11] University of Łódź, 90236 Lodz, Poland
[12] Deutsches Elektronen-Synchrotron (DESY), 15738 Zeuthen, Germany
[13] Institut de Fisica d'Altes Energies (IFAE), The Barcelona Institute of Science and Technology, Campus UAB, 08193 Bellaterra (Barcelona), Spain
[14] Universität Würzburg, 97074 Würzburg, Germany
[15] Università di Padova and INFN, 35131 Padova, Italy
[16] Institute for Space Sciences (CSIC/IEEC), 08193 Barcelona, Spain
[17] Technische Universität Dortmund, 44221 Dortmund, Germany
[18] Finnish MAGIC Consortium, Tuorla Observatory, University of Turku and Astronomy Division, University of Oulu, Oulu, Finland
[19] Unitat de Física de les Radiacions, Departament de Física, and CERES-IEEC, Universitat Autònoma de Barcelona, 08193 Bellaterra, Spain
[20] Universitat de Barcelona, ICC, IEEC-UB, 08028 Barcelona, Spain
[21] Japanese MAGIC Consortium, ICRR, The University of Tokyo, Department of Physics and Hakubi Center, Kyoto University, Tokai University, The University of Tokushima, KEK, Japan
[22] Inst. for Nucl. Research and Nucl. Energy, BG-1784 Sofia, Bulgaria
[23] Università di Pisa, and INFN Pisa, 56126 Pisa, Italy
[24] ICREA and Institute for Space Sciences (CSIC/IEEC), 08193 Barcelona, Spain
[25] Centro Brasileiro de Pesquisas Físicas (CBPF/MCTI), R. Dr. Xavier Sigaud, 150 - Urca, 22290-180 Rio de Janeiro, Brazil
[26] NASA Goddard Space Flight Center, Greenbelt, MD 20771, USA and Department of Physics and Department of Astronomy, University of Maryland, College Park, MD 20742, USA
[27] Humboldt University of Berlin, Institut für Physik Newtonstr. 15, 12489 Berlin, Germany
[28] University of Trieste, Italy
[29] École polytechnique fédérale de Lausanne (EPFL), Lausanne, Switzerland
[30] Max-Planck-Institut fur Kernphysik, PO Box 103980, 69029 Heidelberg, Germany
[31] Japanese MAGIC Consortium, Japan
[32] Finnish Centre for Astronomy with ESO (FINCA), Turku, Finland
[33] INAF-Trieste and Dept. of Physics & Astronomy, University of Bologna, Italy
[34] ISDC – Science Data Center for Astrophysics, 1290 Versoix (Geneva), Switzerland